Alloy-Free Band Gap Tuning across the Visible Spectrum

Robert A. Makin, Krystal York, and Steven M. Durbin*
Department of Electrical and Computer Engineering, Western Michigan University, Kalamazoo, Michigan 49008, USA

Nancy Senabulya, James Mathis, and Roy Clarke
Applied Physics, University of Michigan, Ann Arbor, Michigan 48109, USA

Nathaniel Feldberg and Patrice Miska
Université de Lorraine, CNRS, IJL, F-54000 Nancy, France

Christina M. Jones
Applied Physics, University of Michigan, Ann Arbor, Michigan 48109, USA
and Materials Science and Engineering, University of Michigan, Ann Arbor, Michigan 48109, USA

Zihao Deng, Logan Williams, and Emmanouil Kioupakis
Materials Science and Engineering, University of Michigan, Ann Arbor, Michigan 48109, USA

Roger J. Reeves
School of Physical and Chemical Sciences, University of Canterbury, Christchurch 8140, New Zealand

(Received 11 April 2018; revised manuscript received 16 December 2018; published 27 June 2019)

We present evidence, from theory and experiment, that $ZnSnN_2$ and $MgSnN_2$ can be used to match the band gap of InGaN without alloying—by exploiting cation disorder in a controlled fashion. We base this on the determination of S, the long-range order parameter of the cation sublattice, for a series of epitaxial thin films of $ZnSnN_2$ and $MgSnN_2$ using three different techniques: x-ray diffraction, Raman spectroscopy, and *in situ* electron diffraction. We observe a linear relationship between S^2 and the optical band gap of both $ZnSnN_2$ (1.12–1.98 eV) and $MgSnN_2$ (1.87–3.43 eV). The results clearly demonstrate the correlation between controlled heterovalent cation ordering and the optical band gap, which applies to a broad group of emerging ternary heterovalent compounds and has implications for similar trends in other material properties besides the band gap.

DOI: 10.1103/PhysRevLett.122.256403

Growing concern regarding the future supply of indium and gallium is fueling the search for new semiconductors capable of serving as suitable alternatives to existing materials [1,2]. Given the pervasiveness of the III-nitride family, especially in visible and short-wavelength optoelectronic device applications, analogous indium- and gallium-free compounds with band gap energies in the range of ~1.5–3.5 eV are of key interest. From both economic and ecological perspectives, semiconductor compounds based on Zn, Mg, and Sn are extremely attractive: These three metals are significantly less expensive than In and Ga, they benefit from a mature recycling infrastructure [3], and Zn and Mg are considered earth-abundant elements. $ZnSnN_2$ and $MgSnN_2$, both ternary heterovalent semiconductors, represent potentially viable replacements for commercially important $Ga_xIn_{1-x}N$ alloys. Recently, $ZnSnN_2$ has begun to attract interest as an earth-abundant element semiconductor with potential for photovoltaic device applications [4–9]. At the opposite end of the optical spectrum, $MgSnN_2$—the synthesis of which has not previously been reported—is predicted to have a band gap of 3.43 eV and, thus, represents a potential sustainably sourced semiconductor alternative to GaN for light-emitting diodes and other device applications [10,11].

Compared to their binary analogs, ternary heterovalent semiconductors, such as $ZnSnN_2$ and $MgSnN_2$, have an additional degree of freedom accessible through the symmetry of the cation sublattice, which can be quantified by an order parameter, S. With a perfectly ordered cation sublattice, i.e., the respective column-II and Sn atoms occupying their equilibrium positions ($S = 1$), $ZnSnN_2$ and $MgSnN_2$ belong to the $Pna2_1$ space group. At the opposite extreme ($S = 0$), where each cation site is populated by either the respective column-II or Sn atom with equal probability, the unit cell experiences a reduction in volume and a corresponding increase in symmetry—and the orthorhombic superlattice is reduced to the underlying wurtzite structure. Between these two end points, the lattice can be viewed as a mixture of the orthorhombic and wurtzite structures. The change in the local bonding

environment caused by disorder has previously been shown, in the case of heterovalent materials, to cause a variation of the band gap [12], albeit modest in those cases, which has been treated as an anomaly rather than a method of band gap engineering.

In this Letter, we present theoretical and experimental evidence that by exploiting cation ordering in a controlled fashion we obtain unprecedented band gap variations (on the order of 1 eV) for these two II-IV-N_2 compounds. Furthermore, the range of band gap variation matches that of InGaN without the need for alloying. We detail the methodology for quantifying the degree of cation sublattice ordering through three independent techniques and demonstrate that it is strongly correlated to the band gap. These techniques, along with the control of the band gap through the ordering of the cation sublattice, apply not only to these two materials, but to the larger class of ternary heterovalent materials currently being investigated such as perovskites and chalcopyrites [13–19]. Additionally, we propose that other material characteristics, such as thermal conductivity and nonlinear optical properties, may also show a similar dependence on the order parameter, opening new routes to designing enhanced-performance materials.

Historically, disorder-order transformations in binary material systems are well-studied phenomena, dating back to the case of $CuAu_3$ [20–22]. The most common method for quantifying the degree of ordering is the long-range order parameter S, defined as $S = r_\alpha + r_\beta - 1$, where, in this case, r_α is the fraction of column-II sites occupied by column-II atoms and r_β is the fraction of Sn sites occupied by Sn atoms [23]. Since the samples in this study are stoichiometric, the fraction of Sn on Zn (or Mg) sites must be equal to the fraction of Zn (or Mg) on Sn sites, and, thus, $r_\alpha = r_\beta \equiv r$. Experimentally, S is most often determined with x-ray diffraction measurements through the relative intensity of superlattice reflections whose structure factors depend upon S.

To explore the influence of the cation sublattice ordering on the band gap, we varied growth parameters (using plasma-assisted molecular beam epitaxy) over a series of six stoichiometric thin films, each, of $ZnSnN_2$ and $MgSnN_2$ on yttria-stabilized zirconia substrates [9,24]. Figure 1 shows the θ–2θ plots for the six $ZnSnN_2$ films, where the (002) fundamental reflection and the (210) superlattice reflection have been labeled. Based on the relative intensities of the (002) and (210) reflections, Fig. 1 demonstrates that we were able to obtain films with cation sublattice ordering ranging from almost completely ordered to highly disordered.

Calculating S^2 for a ternary material from θ–2θ plots differs slightly from the binary case. The structure factor of the ternary material will include contributions from the anions, which are independent of the ordering of the cation sublattice. Thus, the magnitude of the structure factor for a superlattice peak in a ternary material has the form

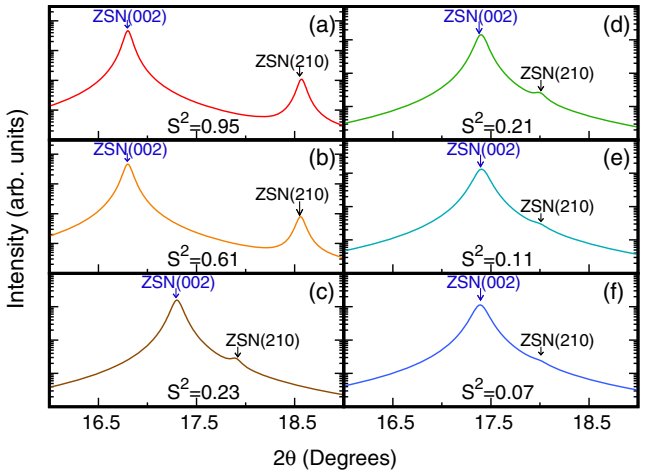

FIG. 1. θ–2θ plots (labeled with the film S^2 value) for six $ZnSnN_2$ films showing the $ZnSnN_2$ (002) and (210) peaks with the substrate peak subtracted. The x-ray diffraction measurements showed no evidence of secondary phases [25].

$|F_{hkl}| = AS + B$, where A is a constant depending on the x-ray scattering factors of the Zn and Sn atoms and B is a constant depending on the x-ray scattering factor of nitrogen. For $ZnSnN_2$, the (210) structure factor was determined to be $|F_{210}| = 37.36S + 4.32$ by performing a linear fit to the $|F_{210}|$ value calculated using VESTA for a range of S values [26]. The order parameter of the samples can then be determined by

$$|F_{210}|^2 = \frac{E_{210}F_{002}^2\left[\frac{1+\cos^2 2\theta_{002}}{2\sin 2\theta_{002}}\right]e^{-2M_{002}}}{E_{002}\left[\frac{1+\cos^2 2\theta_{210}}{2\sin 2\theta_{210}}\right]e^{-2M_{210}}}, \quad (1)$$

where E_{210} is the integrated intensity of the (210) peak, E_{002} is the integrated intensity of the (002) peak, F_{002} is the structure factor for the (002) reflection, $2\theta_{002}$ and $2\theta_{210}$ are the scattering angles for the (002) and (210) reflections, respectively, and M_{210} and M_{002} are the thermal correction factors for the (210) and (002) reflections, respectively [20,21,23]. Consequently, S^2 for the series of films varies from 0.95 to 0.07, which is consistent with tuning between the ordered orthorhombic structure and the disordered wurtzite structure, respectively.

The shift in structure of a ternary heterovalent compound brought on by the disorder of the cation sublattice as observed in x-ray diffraction is also expected to manifest itself in the Raman spectra of $ZnSnN_2$. Orthorhombic $ZnSnN_2$ and $MgSnN_2$ both belong to space group C_{2v}^9. Thus, according to the correlation method, orthorhombic $ZnSnN_2$ and $MgSnN_2$ each have 45 fundamental Raman active modes originating from the four Raman active phonon modes (a_1, a_2, b_1, and b_2) per atom type [27]. The $Pna2_1$ features are most prominent in Figs. 2(b) and 2(d) [28]. The wurtzite unit cells are in space group

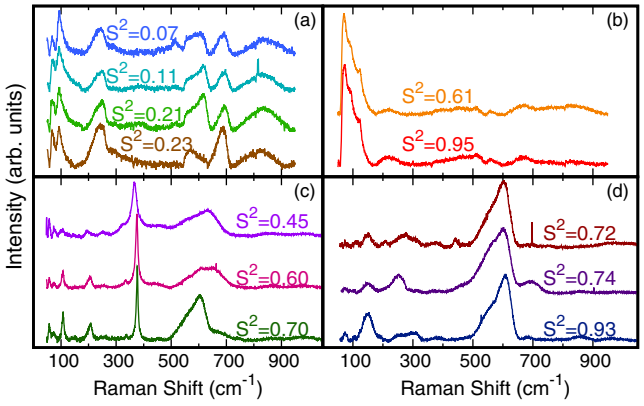

FIG. 2. Measured nonpolarized Raman spectra of $ZnSnN_2$ [(a), (b)] and $MgSnN_2$ films [(c),(d)].

C_{6v}^4 and have two $C_{3v}(2)$ site symmetries, and so wurtzite structures have six fundamental Raman active modes originating from the three Raman active phonon modes (A_1, E_1, and E_2) per atom type (N and column-II or Sn) [27]. The wurtzite unit cell features are most readily identified in the spectrum with S^2 of 0.07 in Fig. 2(a) for $ZnSnN_2$ and in the spectra with an S^2 of 0.45 in Fig. 2(c) for $MgSnN_2$. For partially ordered cation sublattices, a mixture of the modes is expected as has been observed in the closely related material $ZnGeN_2$ [29]. Figure 2(a) shows spectra for the $ZnSnN_2$ films that display such a mixture of orthorhombic and wurtzite peaks.

Following the treatment of Loveluck and Sokoloff for the optical properties of phonon systems with disordered force constants, the Raman spectrum in the lattice region of a partially disordered solid may be written as the sum of the first-order Raman spectrum times S^2 and $(1 - S^2)$ times the Raman spectrum of the disordered spectrum [30,31]. Thus, the order parameters for the films can be found iteratively using a ratio of the integrated intensities of peaks in pairs of samples:

$$\frac{J_{1,S=1}}{J_{2,S=1}} = \frac{S_1^2}{S_2^2}, \qquad \frac{J_{1,S=0}}{J_{2,S=0}} = \frac{1 - S_1^2}{1 - S_2^2}, \tag{2}$$

where J represents integrated intensities of the denoted peak and S_n terms correspond to the order parameter of the associated film. The ordered peak near 70 cm^{-1} and the disordered peak near 100 cm^{-1} were used to calculate S for the $ZnSnN_2$ films. The ordered peak near 150 cm^{-1} and the disordered peak near 100 cm^{-1} were used to calculate S for the $MgSnN_2$ samples. The S values determined by Raman spectroscopy agree to within two decimal places with the values determined via x-ray diffraction (Table I).

S can also be determined through reflection high-energy electron diffraction (RHEED). From x-ray diffraction, we know the $ZnSnN_2$ films have a mixture of two domains present, as evidenced by the presence of both the (002) and (210) reflections, and have seen similar evidence in x-ray diffraction data for $MgSnN_2$. Similar to the (002) x-ray diffraction reflection, the (001) RHEED structure factors for both $ZnSnN_2$ and $MgSnN_2$ are independent of the degree of ordering of the cation sublattice. Because of the similarities of the (210) and (001) planes, the $[1\bar{2}0]$ direction is an axis of symmetry in both the (210) and (001) planes, which results in a superposition of the two RHEED patterns along $[1\bar{2}0]$. From the kinematic RHEED theory, the integrated intensity of a RHEED streak is the product of the initial beam conditions and the structure factor [32]. Thus, the order parameter for a film can be calculated using $|F_{210}|^2 = (E_{210}|F_{001}|^2)/E_{001}$, where E_{210} and E_{001} are the integrated intensity along a (210) and (001) pattern feature, respectively. For calculating the order parameter, the streak profile was taken along the (00) feature of the RHEED pattern and two peaks were fitted (Fig. 3). The order parameters extracted in this manner,

TABLE I. S^2 values and the average r values determined using x-ray diffraction, Raman spectroscopy, and RHEED for $ZnSnN_2$ and $MgSnN_2$.

Film	X ray	Raman	RHEED	r
WPI-90 (ZSN)	0.23	0.23	0.22	0.74
WPI-91 (ZSN)	0.07	0.07	0.07	0.63
WPI-92 (ZSN)	0.61	0.61	0.59	0.89
WPI-93 (ZSN)	0.21	0.21	0.21	0.73
WPI-94 (ZSN)	0.11	0.11	0.12	0.67
WPI-95 (ZSN)	0.95	0.95	0.95	0.99
WPI-124 (MSN)	0.45	0.45	0.45	0.73
WPI-125 (MSN)	0.73	0.72	0.72	0.86
WPI-126 (MSN)	0.60	0.60	0.60	0.80
WPI-127 (MSN)	0.70	0.70	0.70	0.85
WPI-128 (MSN)	0.94	0.93	0.93	0.97
WPI-129 (MSN)	0.74	0.74	0.74	0.87
WPI-141 (MSN)	0.27	0.27	0.27	0.76

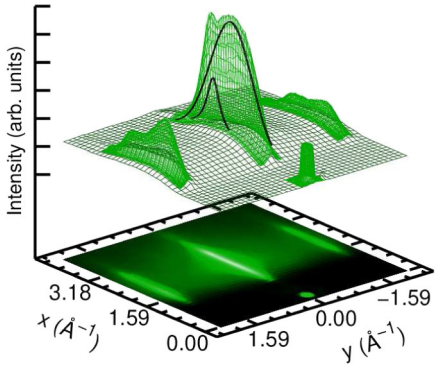

FIG. 3. A representative RHEED image for a $ZnSnN_2$ film shown as an intensity plot projection, along with the two peaks (black) calculated by curve fitting the (00) RHEED streak; the smaller peak is from the (210) plane, and the larger peak is due to the (001) plane.

listed in Table I, are in excellent agreement with the order parameters obtained from x-ray diffraction and Raman spectroscopy.

We now turn to the determination of the optical gap. The direct optical band gaps were determined from absorption edge measurements with the aid of Tauc plots. Theoretical band gaps were obtained with hybrid density functional theory (DFT) calculations implemented using the Vienna *Ab Initio* Simulation Package (VASP) [33–36]. Perdew-Burke-Ernzerhof projector augmented wave pseudopotentials were employed for all atoms [37,38]. The *d* orbitals were included as valence electrons in the Sn pseudopotential. All structures were relaxed, and band gaps were calculated using the Heyd-Scuseria-Ernzerhof (HSE) hybrid functional [39]. Instead of the default 0.25 mixing parameter employed with HSE06, we used a mixing parameter of 0.31 as used by others for $ZnSnN_2$ [40–42]. We employed Brillouin-zone sampling grids of $4 \times 4 \times 4$ for the ordered structure and $1 \times 1 \times 1$ for the partially ordered and disordered structures and a 500 eV plane-wave cutoff for all calculations, which converges energies to below 10 meV. Partially ordered and fully disordered structures were modeled using $2 \times 2 \times 2$ special quasirandom supercells (resulting in 128-atom structures) that minimize the difference of the pair correlation functions compared to random alloys up to a radius of 6 Å [43,44].

Figure 4 shows the optical and theoretical band gaps as a function of S^2. The main feature of Fig. 4 is the strong linear relationship between the band gap and S^2, observable in both the experimental and theoretical band gap values. A linear relationship between S^2 and the band gap has been predicted in binary alloys, such as $Ga_{1-x}In_xP_2$ [45],

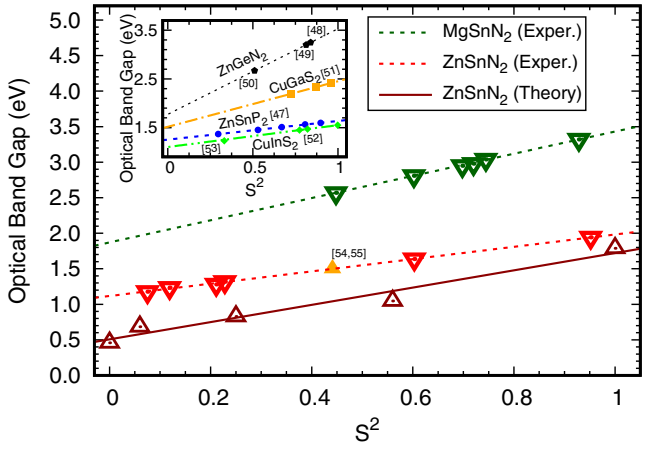

FIG. 4. Optical band gap as a function of S^2. The lines are linear regression fits to their color-coded data: $MgSnN_2$ (green), $ZnSnN_2$ (red), and theoretical $ZnSnN_2$ (dark red). Solid data points have been extracted from the cited references [47–55] as marked. An additional point for $ZnSnN_2$ has been extracted from the literature [54,55]. Inset: Ising model applied to published data for $ZnSnP_2$ [47], $ZnGeN_2$ [48–50], $CuGaS_2$ [51], and $CuInS_2$ [52,53].

although over a significantly smaller band gap range. In their work, Wei *et al.* have showed that a quadratic relationship between *S* and the band gap for semiconductor alloys, and indeed for any lattice property dominated by pair interactions, can be derived using an Ising model with one cation as spin up and the other cation as spin down [45,46]. It is important to note that *S* serves only as a means of expressing the probability of a given site being occupied by the expected atom and not as a source of long-range interactions between atoms. The result is that, for stoichiometric samples, lattice properties where pair interactions are dominant can be expressed as an ensemble average of the properties of the ordered and disordered lattices. Applying this model to the cation sublattice for $ZnSnN_2$,

$$E_{g,S} = E_{g,S=0} + (S^2)[E_{g,S=1} - E_{g,S=0}], \tag{3}$$

where $E_{g,S=0}$ is the band gap of the wurtzite structure, $E_{g,S=1}$ is the band gap of the orthorhombic structure, and $E_{g,S}$ is the band gap of a partially ordered lattice. From a linear fit to the data in Fig. 4, we find $\Delta E_g = 0.865$ eV and $E_{g,S=0} = 1.117$ eV for $ZnSnN_2$ and $\Delta E_g = 1.563$ eV and $E_{g,S=0} = 1.868$ eV for $MgSnN_2$. Also included in Fig. 4 (inset) is the Ising model applied to experimental points extracted from the literature for $ZnSnP_2$ [47], $ZnGeN_2$ [48–50], $CuGaS_2$ [51], and $CuInS_2$ [52,53], which further reinforces the applicability of this analysis to the general family of ternary heterovalent materials.

The major factor influencing the band gap is the motif distribution present in the lattice. A motif consists of four cations surrounding a given V atom. For II-Sn-V materials, there are five possible types of motifs, $(II)_2Sn_2$, $(II)_3Sn$, $(II)Sn_3$, $(II)_4$ and Sn_4. In the ordered state ($S^2 = 1$), only $(II)_2Sn_2$ motifs are present; however, as the long-range order parameter approaches zero ($S^2 \to 0$), other motifs appear in progressively higher amounts. Theoretical results for $ZnSnN_2$ indicate that the motifs lead to the observed trend in band gap reduction as a function of S^2 [56].

The band gap narrowing is due to a decrease in the conduction band minimum (CBM) and an increase in the valence band maximum (VBM). The CBM is mostly derived from the cation *s* states and the VBM from the anion *p* states; thus, it is the influence of motifs on these states that determines the overall effect on the band gap [56,57]. Additionally, it is important to note that in II-Sn-V_2 materials, the $(II)_2Sn_2$ motifs are neutral, since the average charge of the cations is balanced by the nitrogen atom. However, in the other types of motifs, the cation charges are not balanced by the nitrogen atom, and so Sn-rich motifs will be positively charged, while II-rich motifs will be negatively charged.

In the case of Zn and Mg, since Sn has a lower *s* state than the column-II atom and due to the Coulombic attraction of positively charged Sn, the cation *s* level (and, hence, the CBM) will be pushed lower with more

Sn present in the motif. Similarly, the energies of the N $2p$ electrons will be pushed up by Coulombic repulsion from negatively charged Zn-rich motifs; additionally, Zn has higher-energy d levels than Sn, so stronger $p-d$ coupling will also increase the anion p levels (pushing the VBM higher).

The motifs also provide an explanation for the differences among $ZnSnN_2$, $ZnSnP_2$, and $MgSnN_2$ in Fig. 4. The smaller ΔE_g in $ZnSnP_2$ compared to $ZnSnN_2$ can be most likely attributed to the smaller increase in the p level of P compared to the p-level increase of N. The larger band gap change in $MgSnN_2$ compared to $ZnSnN_2$ is most likely due to the larger electronegativity difference between Mg-Sn than Zn-Sn, creating a larger decrease in the CBM than in $ZnSnN_2$, and Mg-rich motifs in $MgSnN_2$ causing a larger shift in the VBM than Zn-rich motifs in $ZnSnN_2$.

In conclusion, we have grown a series of thin films of $ZnSnN_2$ with S^2 values varying from 0.07 to 0.95 and a series of $MgSnN_2$ thin films with S^2 ranging from 0.27 to 0.93. We have calculated the order parameter for the films using measurements from three different techniques with close agreement among the techniques. We propose that the properties of the partially ordered system can be understood in the context of an Ising model. We have validated the linear relationship between the measured optical gap and S^2 predicted by the Ising model for our samples and for four other related compounds. We propose that the other properties of the partially ordered system may also be understood in the context of an Ising model.

Moreover, the range spanned by the cation sublattice ordering of $ZnSnN_2$ and $MgSnN_2$, approximately 1.12–3.43 eV, positions these materials as earth-abundant eco-friendly alternatives to $Ga_xIn_{1-x}N$ alloys. Taking the combined density functional theory calculations and iterative synthesis and characterization results together, the inherent value of this emerging approach for materials design is readily apparent—not only have new materials been realized, but a fundamentally new mechanism has been demonstrated for tuning band gap energies over a large range.

The DFT calculations were supported by the National Science Foundation through Grant No. DMR-1254314 and used resources of the National Energy Research Scientific Computing (NERSC) Center, a Department of Energy Office of Science User Facility supported under Contract No. DEAC0205CH11231. P. M. and N. F. thank the European Regional Development Fund, the Institut Carnot ICEEL, and the Region Lorraine. P. M. thanks the Agence Nationale de la Recherche OPERA project, Grant No. ANR-17-CE05-0022 and the ISITE-LUE program of the UL for funding. X-ray diffraction experiments were performed at sectors 13-BMC (GeoSoilEnviroCARS), and 33-BMC (XSD) at the Advanced Photon Source. Excellent beam line support by P. Eng, J. Stubbs, E. Karapetrova, and the staff of the A. P. S. is gratefully acknowledged. GeoSoilEnviroCARS is supported by the National Science Foundation—Earth Sciences (EAR-0622171) and Department of Energy—Geosciences (DE-FG02-94ER14466). The use of the A. P. S. was supported by the U.S. Department of Energy, Office of Science, Office of Basic Energy Sciences, under Contract No. DE-AC02-06CH11357. Experimental studies of $ZnSnN_2$ were supported in part by the National Science Foundation, Grants No. DMR-1410915 and No. DMR-10006835. Experimental studies of $MgSnN_2$ were supported in part through a grant from the Faculty Research and Creative Activities Award (FRACAA) program of Western Michigan University. Optical measurements were performed through support from the MacDiarmid Institute for Advanced Materials and Nanotechnology.

*steven.durbin@wmich.edu

[1] European Commission, DG Enterprise and Industry, Critical raw materials for the EU (Ad-hoc Working Group on defining critical raw materials), European Commission, 2010, https://ec.europa.eu/growth/tools-databases/eip-raw-materials/en/community/document/critical-raw-materials-eu-report-ad-hoc-working-group-defining-critical-raw.

[2] R. Jaffe, J. Price, M. Hitzman, and F. Slakey, APS News **20**, 4 2011.

[3] J. A. Ober, Mineral Commodity Summaries 2016, technical report, Reston, VA, 2016.

[4] L. Lahourcade, N. C. Coronel, K. T. Delaney, S. K. Shukla, N. A. Spaldin, and H. A. Atwater, Adv. Mater. **25**, 2562 (2013).

[5] F. Kawamura, N. Yamada, M. Imai, and T. Taniguchi, Cryst. Res. Technol. **51**, 220 (2016).

[6] R. Qin, H. Cao, L. Liang, Y. Xie, F. Zhuge, H. Zhang, J. Gao, K. Javaid, C. Liu, and W. Sun, Appl. Phys. Lett. **108**, 142104 (2016).

[7] A. N. Fioretti, A. Stokes, M. R. Young, B. Gorman, E. S. Toberer, A. C. Tamboli, and A. Zakutayev, Adv. Electron. Mater. **3**, 1600544 (2017).

[8] P. C. Quayle, G. T. Junno, K. He, E. W. Blanton, J. Shan, and K. Kash, Phys. Status Solidi B **254**, 1600718 (2017).

[9] N. Feldberg, J. Aldous, W. Linhart, L. Phillips, K. Durose, P. Stampe, R. Kennedy, D. Scanlon, G. Vardar, R. Field III *et al.*, Appl. Phys. Lett. **103**, 042109 (2013).

[10] A. P. Jaroenjittichai and W. R. L. Lambrecht, Phys. Rev. B **94**, 125201 (2016).

[11] K. Kanchiang, T. Cheiwchanchamnangij, Y. Laosiritaworn, S. Pramchu, and A. P. Jaroenjittichai, J. Phys. Conf. Ser. **1144**, 012149 (2018).

[12] S.-H. Wei, L. G. Ferreira, and A. Zunger, Phys. Rev. B **45**, 2533 (1992).

[13] J. Vidal, F. Trani, F. Bruneval, M. A. L. Marques, and S. Botti, Phys. Rev. Lett. **104**, 136401 (2010).

[14] D. D. Sarma, N. Shanthi, S. R. Barman, N. Hamada, H. Sawada, and K. Terakura, Phys. Rev. Lett. **75**, 1126 (1995).

[15] Z. Lebens-Higgins, D. O. Scanlon, H. Paik, S. Sallis, Y. Nie, M. Uchida, N. F. Quackenbush, M. J. Wahila, G. E. Sterbinsky,

D. A. Arena, J. C. Woicik, D. G. Schlom, and L. F. J. Piper, Phys. Rev. Lett. **116**, 027602 (2016).
[16] R. F. Berger, C. J. Fennie, and J. B. Neaton, Phys. Rev. Lett. **107**, 146804 (2011).
[17] M. Sebastian, J. A. Peters, C. C. Stoumpos, J. Im, S. S. Kostina, Z. Liu, M. G. Kanatzidis, A. J. Freeman, and B. W. Wessels, Phys. Rev. B **92**, 235210 (2015).
[18] X.-W. Yan, M. Gao, Z.-Y. Lu, and T. Xiang, Phys. Rev. Lett. **106**, 087005 (2011).
[19] M. H. Upton, Y. Choi, H. Park, J. Liu, D. Meyers, J. Chakhalian, S. Middey, J.-W. Kim, and P. J. Ryan, Phys. Rev. Lett. **115**, 036401 (2015).
[20] J. M. Cowley, J. Appl. Phys. **21**, 24 (1950).
[21] Z. W. Wilchinsky, J. Appl. Phys. **15**, 806 (1944).
[22] D. T. Keating and B. E. Warren, J. Appl. Phys. **22**, 286 (1951).
[23] B. Warren, *X-Ray Diffraction*, Dover Books on Physics (Dover, New York, 2012), pp. 357–437.
[24] R. A. Makin, N. Senabulya, J. Mathis, N. Feldberg, P. Miska, R. Clarke, and S. M. Durbin, J. Vac. Sci. Technol. B **35**, 02B116 (2017).
[25] N. Senabulya, N. Feldberg, R. A. Makin, Y. Yang, G. Shi, C. M. Jones, E. Kioupakis, J. Mathis, R. Clarke, and S. M. Durbin, AIP Adv. **6**, 075019 (2016).
[26] K. Momma and F. Izumi, J. Appl. Crystallogr. **44**, 1272 (2011).
[27] W. Fateley, *Infrared and Raman Selection Rules for Molecular and Lattice Vibrations: The Correlation Method* (Wiley-Interscience, New York, 1972).
[28] See Supplemental Material at http://link.aps.org/supplemental/10.1103/PhysRevLett.122.256403 for details of Raman experimental set-up, Tauc plots, RHEED images, and θ–2θ x-ray diffraction plots.
[29] T. J. Peshek, T. R. Paudel, K. Kash, and W. R. L. Lambrecht, Phys. Rev. B **77**, 235213 (2008).
[30] J. Loveluck and J. Sokoloff, J. Phys. Chem. Solids **34**, 869 (1973).
[31] T. Y. Shen, S. S. Mitra, H. Prask, and S. F. Trevino, Phys. Rev. B **12**, 4530 (1975).
[32] A. Ichimiya and P. Cohen, *Reflection High-Energy Electron Diffraction* (Cambridge University Press, Cambridge, England, 2004), pp. 130–153.
[33] G. Kresse and J. Hafner, Phys. Rev. B **47**, 558 (1993).
[34] G. Kresse and J. Hafner, Phys. Rev. B **49**, 14251 (1994).
[35] G. Kresse and J. Furthmller, Comput. Mater. Sci. **6**, 15 (1996).
[36] G. Kresse and J. Furthmüller, Phys. Rev. B **54**, 11169 (1996).
[37] J. P. Perdew, K. Burke, and M. Ernzerhof, Phys. Rev. Lett. **77**, 3865 (1996).
[38] G. Kresse and D. Joubert, Phys. Rev. B **59**, 1758 (1999).
[39] J. Heyd, G. E. Scuseria, and M. Ernzerhof, J. Chem. Phys. **118**, 8207 (2003).
[40] P. Narang, S. Chen, N. C. Coronel, S. Gul, J. Yano, L. Wang, N. S. Lewis, and H. A. Atwater, Adv. Mater. **26**, 1235 (2014).
[41] S. Chen, P. Narang, H. A. Atwater, and L. Wang, Adv. Mater. **26**, 311 (2014).
[42] T. Wang, C. Ni, and A. Janotti, Phys. Rev. B **95**, 205205 (2017).
[43] A. Zunger, S.-H. Wei, L. G. Ferreira, and J. E. Bernard, Phys. Rev. Lett. **65**, 353 (1990).
[44] A. van de Walle, P. Tiwary, M. de Jong, D. Olmsted, M. Asta, A. Dick, D. Shin, Y. Wang, L.-Q. Chen, and Z.-K. Liu, CALPHAD: Comput. Coupling Phase Diagrams Thermochem. **42**, 13 (2013).
[45] S. Wei, D. B. Laks, and A. Zunger, Appl. Phys. Lett. **62**, 1937 (1993).
[46] D. B. Laks, S.-H. Wei, and A. Zunger, Phys. Rev. Lett. **69**, 3766 (1992).
[47] S. Nakatsuka and Y. Nose, J. Phys. Chem. C **121**, 1040 (2017).
[48] K. Du, C. Bekele, C. C. Hayman, J. C. Angus, P. Pirouz, and K. Kash, J. Cryst. Growth **310**, 1057 (2008).
[49] R. Viennois, T. Taliercio, V. Potin, A. Errebbahi, B. Gil, S. Charar, A. Haidoux, and J. C. Tdenac, Mater. Sci. Eng. B **82**, 45 (2001).
[50] W. L. Larson, H. P. Maruska, and D. A. Stevenson, J. Electrochem. Soc. **121**, 1673 (1974).
[51] P. Prabukanthan and R. Dhanasekaran, Cryst. Growth Des. **7**, 618 (2007).
[52] A. M. Martinez, L. G. Arriaga, A. M. Fernndez, and U. Cano, Mater. Chem. Phys. **88**, 417 (2004).
[53] Y. Qi, Q. Liu, K. Tang, Z. Liang, Z. Ren, and X. Liu, J. Phys. Chem. C **113**, 3939 (2009).
[54] P. C. Quayle, K. He, J. Shan, and K. Kash, MRS Commun. **3**, 135 (2013).
[55] P. C. Quayle, E. W. Blanton, A. Punya, G. T. Junno, K. He, L. Han, H. Zhao, J. Shan, W. R. L. Lambrecht, and K. Kash, Phys. Rev. B **91**, 205207 (2015).
[56] J. Ma, H.-X. Deng, J.-W. Luo, and S.-H. Wei, Phys. Rev. B **90**, 115201 (2014).
[57] S. Lany, A. N. Fioretti, P. P. Zawadzki, L. T. Schelhas, E. S. Toberer, A. Zakutayev, and A. C. Tamboli, Phys. Rev. Mater. **1**, 035401 (2017).